Explosive connectivity and mechanical rigidity in cubic lattice structures

Trenton Lau [*] and Gary P. T. Choi [†]
Department of Mathematics, The Chinese University of Hong Kong, Hong Kong, China

(Received 4 November 2025; accepted 19 October 2026; published 6 November 2026)

We study explosive connectivity and mechanical rigidity in three-dimensional cubic lattice structures under Achlioptas-type product-rule dynamics. Our work combines extensive numerical simulation with a theoretical framework based on rigorous finite-size scaling. Using massive-scale simulations up to $L = 192$ ($N \approx 7 \times 10^6$) with 20 000 independent realizations, we demonstrate that for $k \geqslant 8$, the peak susceptibility scales with an exponent of $\gamma = 1.000$, and the maximum single-step jump stabilizes at a macroscopic fraction. This confirms that while the transition is continuous in the infinite thermodynamic limit, it exhibits the exact finite-size scaling signatures of a first-order discontinuity in finite physical systems. For rigidity, we discover numerically that for richly connected hosts, increasing the number of choices k optimally enhances the efficiency of rigidification. To explain this phenomenon, we propose a theoretical model centered on a conditional progress function that links an edge's local product-rule score to its global mechanical utility. We show that while local rigidification efficiency monotonically increases, the global rigidity gap exhibits a "Goldilocks" minimum at intermediate k due to the emergence of maximally floppy, treelike components at large k. Altogether, our work provides new insights into the relationship between local dynamics and global connectivity and rigidity in cubic lattice structures via both theory and computation.

DOI: 10.1103/1fr3-bbxr

I. INTRODUCTION

Percolation is a canonical framework for phase transitions in disordered media [1,2] and has found widespread applications in science and engineering [3–7]. Competitive link-selection rules in Achlioptas-type processes can produce explosive phase transitions on both random graphs and regular lattice networks [8–13]. While early studies suggested a discontinuous (first-order) transition, rigorous mathematical proofs [14] and large-scale simulations [15–20] have established that for any fixed number of choices, the transition is continuous in the thermodynamic limit, albeit with anomalous scaling behaviors. However, for finite systems typical of mechanical assemblies and metamaterials, the transition often remains indistinguishable from a discontinuity.

Mechanical rigidity percolation probes the emergence of generic infinitesimal rigidity [21–23] and can be efficiently tested by the two-dimensional (2D) pebble game [24,25]. Note that while the three-dimensional (3D) pebble game provides a necessary condition for rigidity, it is not always sufficient; however, it serves as a powerful heuristic for large networks [26]. In recent years, there has been increasing interest in the explosive rigidity percolation in various 2D systems, including origami structures [27,28] and kirigami structures [29]. Some works have also studied the explosive percolation of physical systems in different dimensions [18,30]. In particular, deterministic and stochastic approaches have been developed for controlling the connectivity and rigidity of 3D cubic and prismatic assemblies [31].

In physical and biological systems, the emergence of global mechanical stability is rarely a purely random process. Instead, it is governed by competitive, history-dependent assembly pathways. For instance, in the self-assembly of mechanical metamaterials or the aggregation of attractive particulate gels, the system can undergo rapid, random aggregation (akin to fast quenching), which typically yields tenuous, "floppy" dendritic networks. Conversely, slower, energetically favorable pathways (akin to annealing) allow the system to explore local configurations, avoiding premature, inefficient connections and ultimately achieving global rigidity with fewer redundant bonds. To model this competition between local selection rules and global mechanical stability, we employ the Achlioptas process with a choice parameter, k. Physically, k acts as a *kinetic dial* or a proxy for the thermodynamic assembly protocol: $k = 1$ corresponds to standard random percolation (fast quenching), while $k > 1$ grants the system a "choice" to suppress the growth of the giant component, favoring the merging of smaller, isolated clusters. However, establishing a direct relationship between such a local choice mechanism and the *global* connectivity and rigidity remains highly challenging. In particular, the mechanical utility of a potential bond depends on the complex, nonlocal structure of the entire existing network, and it is not guaranteed that a simple local rule can lead to monotonic improvements in global stability. Motivated by these challenges, this paper combines theory and computation to study the explosive connectivity and mechanical rigidity in 3D cubic

[*]Contact author: trentonlau@link.cuhk.edu.hk
[†]Contact author: ptchoi@cuhk.edu.hk

Published by the American Physical Society under the terms of the Creative Commons Attribution 4.0 International license. Further distribution of this work must maintain attribution to the author(s) and the published article's title, journal citation, and DOI.

lattice structures. Specifically, by performing comprehensive numerical simulations under an Achlioptas process, we analyze connectivity and rigidity in 3D cubic lattice structures. Using the nearest-neighbor (NN) model as a control and the Intra cube model as the target system, we uncover several key phenomena. We then develop a series of theoretical models to explain the phenomena. Our main contributions include the following:

(1) We numerically characterize the explosive connectivity transition. While the onset of anomalous finite-size scaling (a merger cascade) begins at $k = 2$, we demonstrate that for $k \geqslant 8$, the transition width collapses inversely with system volume, and the susceptibility scaling exactly matches a first-order discontinuity ($\gamma = 1.000$).

(2) For the richly connected Intra model, we observe a significant rigidity-connectivity gap that shrinks dramatically to a global minimum at an intermediate k before widening slightly as k becomes very large.

(3) We develop a theoretical framework to explain these observations. Specifically, we derive the existence of merger-cascade windows that drive the abrupt growth of the giant component in finite systems.

(4) We introduce a *conditional progress function* to explain this optimal rigidification efficiency. We show that this local efficiency is a direct consequence of two physically motivated assumptions, for which we provide strong supporting evidence using tractable random subgraph models.

II. PRELIMINARIES AND SYSTEM SETUP

In this work, we study explosive connectivity and mechanical rigidity in 3D cubic lattice structures. We build these structures progressively using a competitive link-selection scheme known as an Achlioptas process. This section introduces our core physical models and the essential theoretical concepts. For a comprehensive list of foundational definitions from graph theory, rigidity theory, and probability theory, the reader is referred to Sec. S1 of the Supplemental Material [32].

A. Host geometries: The NN and Intra models

We focus on two host models of 3D cubic lattice structures, namely, the *NN* (Shell 1) model and the *Intra* (S1–S3) model (see Fig. 1 for visualizations of their respective configurations).

Definition 1 (NN unit cell graph). The NN unit cell graph $G_{\mathrm{NN}}^{\mathrm{unit}} = (V_{\square}, E_{\mathrm{NN}})$ has a vertex set $V_{\square} = \{0, 1\}^3$ (the eight cube corners) and an edge set E_{NN} consisting of all pairs $\{u, v\}$ with $d^2(u, v) = 1$. Here, $d(u, v) = \sqrt{(x_1 - x_2)^2 + (y_1 - y_2)^2 + (z_1 - z_2)^2}$ is the Euclidean distance between two points $u = (x_1, y_1, z_1)$ and $v = (x_2, y_2, z_2)$.

As shown in Fig. 1(a), the NN unit cell graph contains exactly the 12 axis-aligned edges of the cube, and hence $|E_{\mathrm{NN}}| = 12$.

Definition 2 (Intra unit cell graph). The Intra cube unit cell graph $G_{\mathrm{intra}}^{\mathrm{unit}} = (V_{\square}, E_{\mathrm{intra}})$ has the same vertex set $V_{\square}$, and the edge set E_{intra} consisting of all pairs $\{u, v\}$ with $d^2(u, v) \in \{1, 2, 3\}$.

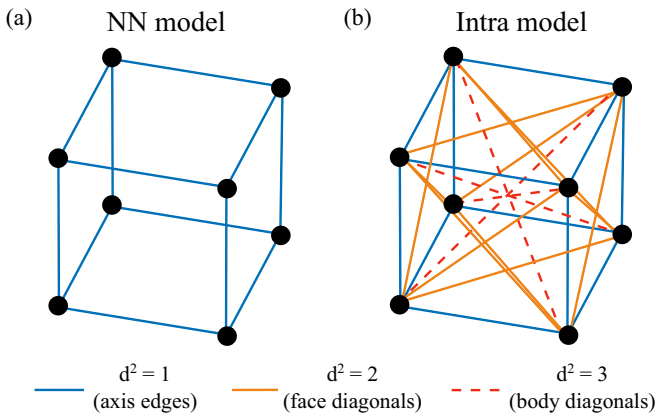


FIG. 1. The two 3D vertex models considered in this study. (a) The NN model. (b) The Intra cube model.

As shown in Fig. 1(b), for the Intra unit cell graph, E_{intra} contains the 12 axis edges ($d^2 = 1$), the 12 face diagonals ($d^2 = 2$), and the 4 body diagonals ($d^2 = 3$). Therefore, $|E_{\mathrm{intra}}| = 12 + 12 + 4 = 28$.

Using the above unit cell graph, we can consider a 3D cubic lattice structure with size $(L + 1) \times (L + 1) \times (L + 1)$ for any $L \geqslant 1$. By simple counting, we can see that there are in total $L(L + 1)(L + 1) \times 3 = 3L^3 + 6L^2 + 3L$ edges, $2L^2(L + 1) \times 3 = 6L^3 + 6L^2$ face diagonals, and $4L^3$ body diagonals. Therefore, denoting the total number of potential edges for the structure as M, for the NN model we have

$$M = 3L^3 + 6L^2 + 3L,$$

while for the Intra model we have

$$\begin{aligned} M &= (3L^3 + 6L^2 + 3L) + (6L^3 + 6L^2) + (4L^3) \\ &= 13L^3 + 12L^2 + 3L. \end{aligned}$$

B. The k-choice Achlioptas process

Starting with the vertices in a 3D cubic lattice structure without any links, we study the change in connectivity and rigidity of the system if we progressively add the links based on either of the two host models. In particular, we are interested in how the choice of the links and the type of the host model affect the rigidity and connectivity throughout the entire process. In this study, we will consider adding the links both stochastically and via an Achlioptas process (see Fig. 2 for an illustration). In each discrete time step, the parameter k represents the number of randomly sampled options from which one optimal choice is made.

Below, we define the core selection mechanism based on component sizes.

Definition 3 (Product score). At any step t of a graph evolution process, let G^{t-1} be the current graph. For any candidate edge $e = \{u, v\}$ not yet in G^{t-1}, its *product score* is defined as

$$s_t(e) := |C_{G^{t-1}}(u)| \times |C_{G^{t-1}}(v)|,$$

where $|C_{G^{t-1}}(x)|$ is the size of the connected component containing vertex x in the graph G^{t-1}.

With this, we can now define the Achlioptas process used in this study.

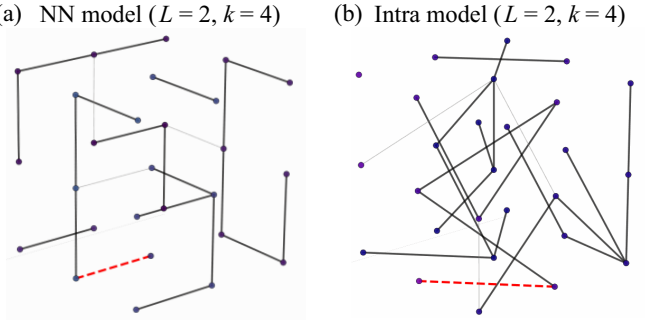


FIG. 2. An illustration of the k -choice Achlioptas process on an intermediate state of a cubic lattice structure with $L = 2$ and $k = 4$. (a) The NN model. (b) The Intra model. The existing edges from the previous states are in black. At the current state, four candidate edges (in gray and red) are sampled, and the one that minimizes the product score is selected (red).

Definition 4 (Product rule with k choices). Let E be the set of all possible edges in a graph. Fix $k \in \{1, 2, \ldots\}$. At each step $t = 1, 2, \ldots$, we perform the following:

(1) Sample k distinct candidate edges $S_t = \{e_{t,1}, \ldots, e_{t,k}\}$ uniformly at random without replacement from the remaining edges $E \setminus E^{t-1}$.

(2) Compute the product score $s_t(e)$ for each $e \in S_t$ using the current graph G^{t-1}.

(3) Select one edge $e_t \in S_t$ that minimizes $s_t(e)$ (if several edges tie for the minimum, break ties uniformly at random).

(4) Set $E^t := E^{t-1} \cup \{e_t\}$.

The sequence $(G^t)_{t \geqslant 0}$ obtained this way is the k-choice product-rule Achlioptas process.

C. Fundamentals of mechanical rigidity

To analyze the mechanical rigidity of the cubic lattice structures, we now formalize the key concepts from rigidity theory [51]. These definitions establish the mathematical basis for quantifying when a framework of vertices and edges is stable against infinitesimal deformations.

Definition 5 (Rigidity matrix). An *infinitesimal flex* of a framework (G, P), where $G = (V, E)$ is a graph and $P : V \to \mathbb{R}^d$ assigns to each vertex $v \in V$ a position $p_v \in \mathbb{R}^d$, is an assignment of velocities δP to the vertices such that the length of any edge $\{u, v\} \in E$ does not change to first order. This is expressed by the linear constraints

$$(p_u - p_v) \cdot (\delta p_u - \delta p_v) = 0.$$

These constraints can be written as a linear system $R(P)\,\delta P = 0$, where $R(P)$ is the *rigidity matrix* of size $|E| \times 3|V|$. The row corresponding to edge $\{u, v\}$ contains the vectors $(p_u - p_v)$ and $(p_v - p_u)$ in the columns associated with vertices u and v, respectively, and zeros elsewhere. The space of all solutions, the *infinitesimal flex space*, is the kernel $\ker R(P) \subseteq \mathbb{R}^{3|V|}$.

Definition 6 (Trivial motions and floppy modes). In 3D, any framework admits a six-dimensional space of *trivial* infinitesimal motions corresponding to three global translations and three global rotations of the entire structure. A motion is *nontrivial* if it deforms the framework. We define the number of independent nontrivial motions, or *floppy modes*, as

$$f(G, P) \;=\; \dim \ker R(P) - 6.$$

A framework (G, P) is *infinitesimally rigid* if it has no floppy modes, i.e., if $f(G, P) = 0$. This property is often referred to as local rigidity, and it is distinct from the stronger condition of *global rigidity*, where a generic framework is uniquely determined by its edge lengths up to isometries. The study of global rigidity has deep connections to graph connectivity and unique reconstruction from distance data [52].

Definition 7 (Generic placements and generic rigidity). A property holds for *generic placements* if it holds for all vertex positions P outside a specific lower-dimensional algebraic variety (a set of measure zero). A graph G is *generically rigid* if the framework (G, P) is infinitesimally rigid for all generic placements P.

For the NN and Intra host models introduced previously, note that the *Maxwell count* for generic 3D rigidity states that a necessary condition for a graph $G = (V, E)$ to be generically infinitesimally rigid in 3D is

$$|E| \;\geqslant\; 3|V| - 6.$$

In particular, applying the Maxwell count to the unit cell graph, we have

$$3|V| - 6 \;=\; 3(8) - 6 \;=\; 24 - 6 \;=\; 18.$$

It follows that the NN unit cell graph (12 edges) can never be rigid.

While the Maxwell count is necessary, it is not sufficient for rigidity in three dimensions. This stands in contrast to the two-dimensional case, where a complete combinatorial characterization is given by Laman's Theorem [53]: A graph is minimally rigid in 2D if and only if $|E| = 2|V| - 3$ and for every subgraph with $|V'| \geqslant 2$ vertices, $|E'| \leqslant 2|V'| - 3$. It provides a purely combinatorial condition and is a cornerstone of the modern matroid-theoretic approach to rigidity [54]. The absence of such a complete characterization for $d \geqslant 3$ implies that combinatorial algorithms [like the (3, 6) pebble game [24,25]] provide a *necessary* but not strictly *sufficient* condition for generic rigidity. Recently, there have been significant algorithmic breakthroughs in exact rigidity analysis [55,56]. For instance, novel integrations of the pebble game with Newman-Ziff approaches and exact cluster-merging theorems have achieved near-linear time complexity for exact 2D rigidity percolation [55]. Furthermore, dynamic event-based ensemble approaches have recently been formulated to efficiently track rigid cluster evolutions and cascade mergers in 2D systems [56]. However, as is well known in rigidity theory [23,26], the exact determination of generic rigid clusters in three (or more) dimensions remains a crucial computational and theoretical bottleneck. Furthermore, on finite 3D cubic lattices with open boundaries, the strict algorithmic enforcement of the $3|V| - 6$ condition encounters "first-edge" initialization paradoxes and can become trapped by local overconstrained subgraphs or boundary anomalies.

To circumvent these combinatorial traps while capturing the macroscopic mechanical transition, we measure *relaxed rigidity*. In this relaxed framework, an edge is deemed mechanically independent if it bridges two topologically

disconnected components (thereby removing a relative translational degree of freedom), or if it successfully consumes a pebble under the relaxed Intra component pebble conservation rules. This heuristic successfully tracks the bulk rigidification process without being artificially halted by localized boundary anomalies.

Assumption 1 (Generic placements and tie avoidance). All statements regarding rigidity in this paper are made for generic placements P of the vertices V_L in $\mathbb{R}^3$. This measure-one assumption ensures that any lack of rigidity is due to the combinatorial structure of the graph rather than a nongeneric, degenerate alignment of vertices.

D. Quantifying connectivity and mechanical rigidity

To analyze the change in connectivity, we consider the connected components in the cubic lattice structures. For a system of a given linear size L, we denote $N = (L+1)^3$ as the total number of vertices and M as the total number of potential edges for the host graph.

Definition 8 (Connected components and sizes). For a graph $H = (V, F)$, its (vertex) connected components are the maximal subsets of vertices within which every pair is connected by a path using edges from F. For a vertex v, write $C_H(v)$ for the component of v in H and $|C_H(v)|$ for its size (number of vertices).

In particular, we denote $S_{\max}$ as the number of vertices in the largest connected component.

A key quantity for characterizing the connectivity transition is the susceptibility. It is defined as the mean size of the component to which a randomly chosen vertex belongs. Let the system have components C_i of size (number of vertices) s_i. A vertex ρ chosen uniformly at random belongs to a specific component C_i with probability s_i/N. The expected component size is therefore equivalent to the second moment of the cluster size distribution:

$$\mathbb{E}[|C(\rho)|] = \sum_{\text{all clusters } i} s_i \times \frac{s_i}{N} = \frac{1}{N} \sum_{\text{all clusters } i} s_i^2.$$

Based on this, we define two distinct susceptibility measures for theoretical and numerical purposes:

Definition 9 (Susceptibility measures). Let s_i be the size of the ith connected component and $S_{\max}$ be the size of the largest component.

(1) The *inclusive susceptibility*, denoted by χ_L, is given by

$$\chi_L(p) = \frac{1}{N} \sum_{\text{all clusters } i} s_i^2.$$

This quantity is mathematically nondecreasing with link density p and is used in our theoretical proofs.

(2) The *exclusive susceptibility* (of finite clusters), denoted by χ'_L, is defined by summing only over clusters that are not the largest one:

$$\chi'_L(p) = \frac{1}{N} \sum_{i \neq \max} s_i^2 = \chi_L(p) - \frac{S_{\max}^2}{N}.$$

This quantity exhibits a sharp peak at the percolation threshold p_c and is therefore the standard tool for numerically locating the transition point [1].

(3) The *peak susceptibility*, denoted by $\chi'_{L,\max}$, is the maximum value of the exclusive susceptibility over the entire link density range:

$$\chi'_{L,\max} := \max_p \chi'_L(p).$$

This quantity is utilized in our finite-size scaling (FSS) analysis to locate transition points.

The detailed analysis of the full order parameter distribution, from which such moments are derived, provides a powerful and refined method for characterizing critical phenomena and improving numerical estimates in finite-size scaling, as pioneered for the Ising model [57].

To analyze the efficiency of the rigidification process, we must quantify the contribution of each added edge. The rigidity of a framework (G, P) is determined by the rank of its rigidity matrix, $R(P)$. We adopt the following definitions:

Definition 10 (Rank gain and edge redundancy). Let (G, P) be a framework. For an edge $e \notin E(G)$, its *rank gain* is defined as

$$\text{rgain}(e) := \text{rank}(R_P(G+e)) - \text{rank}(R_P(G)).$$

For a generic placement, the rank gain is either 0 or 1. An edge e is *nonredundant* if $\text{rgain}(e) = 1$ and *redundant* if $\text{rgain}(e) = 0$.

Definition 11 (Single-step progress). We define the single-step progress toward rigidity at step t, $\Delta\Phi_t$, as the rank gain of the edge e_t added at that step: $\Delta\Phi_t = \text{rgain}(e_t)$. The total number of redundant edges added by time T is therefore $N_{\text{red}}(T) = T - \sum_{t=1}^{T} \Delta\Phi_t$.

Remark. In numerical simulations of finite open lattices, the strict exact calculation of generic rank gain is heavily obscured by boundary floppy modes. Therefore, the single-step progress $\Delta\Phi_t$ is operationally measured using the standard (3, 6) pebble game. We utilize this as a "relaxed" heuristic: Because the algorithm successfully identifies intercomponent degrees of freedom while gracefully handling internal redundancy, it serves as a highly robust, scale-invariant combinatorial proxy for the bulk theoretical rank gain, bypassing the severe boundary anomalies of open finite lattices.

To formalize the critical transition points, we first define the order parameter for rigidity, analogous to the one for connectivity, and then define the thresholds in the thermodynamic limit.

Definition 12 (Critical thresholds). Let $G = (V, E)$ be a graph.

(1) The *connectivity order parameter* for a system of size N at density p is the expected fraction of vertices in the largest connected component:

$$P_N(p) := \mathbb{E}\left[\frac{S_{\max}(G^{\lfloor pM \rfloor})}{N}\right].$$

(2) The *largest rigid cluster* of G, denoted by $R_{\max}(G)$, is a maximal generically rigid subgraph of G with the largest number of vertices. We define its size as $S_{\max}^{\text{rigid}}(G) := |V(R_{\max}(G))|$.

(3) The *rigidity order parameter* for a system of size N at density p is the expected fraction of vertices in the largest

rigid cluster:

$$P_N^{\text{rigid}}(p) := \mathbb{E}\left[\frac{S_{\max}^{\text{rigid}}(G^{\lfloor pM \rfloor})}{N}\right].$$

(4) The *connectivity threshold*, p_c^{conn}, is the infimum of densities where the connectivity order parameter $P_N(p)$ is nonzero in the thermodynamic limit ($N \to \infty$):

$$p_c^{\text{conn}} := \inf\{p \in [0,1] | \lim_{N\to\infty} P_N(p) > 0\}.$$

(5) The *rigidity threshold*, p_c^{rigidity}, is the infimum of densities where the rigidity order parameter is nonzero in the thermodynamic limit:

$$p_c^{\text{rigidity}} := \inf\{p \in [0,1] | \lim_{N\to\infty} P_N^{\text{rigid}}(p) > 0\}.$$

In numerical simulations on finite systems, these thresholds are estimated by the location of the peaks of their corresponding susceptibilities.

It is well known that rigidity implies connectivity [51]. Therefore, the rigidity threshold can be no lower than the connectivity threshold. This allows us to define the *rigidity-connectivity gap*:

Definition 13 (Rigidity-connectivity gap). The rigidity-connectivity gap Δp_c is defined as the difference between the rigidity threshold and the connectivity threshold:

$$\Delta p_c = p_c^{\text{rigidity}} - p_c^{\text{conn}} \geqslant 0.$$

This gap quantifies the additional link density required to rigidify the system after a giant connected component has already formed and will be a central quantity measured in our numerical results.

III. NUMERICAL RESULTS AND ANALYSIS

To investigate the emergence of connectivity and rigidity, we conducted massive-scale numerical simulations on 3D cubic lattices of size $(L+1)\times(L+1)\times(L+1)$ for L up to 192, analyzing both the NN (Shell 1) and Intra (S1–S3) models with choice parameter k from 1 to 32. Here, to balance physical accuracy with computational feasibility, we adopt a two-tiered numerical strategy. Sweeping 32 distinct values of the choice parameter k while evaluating the 3D relaxed pebble game over 20 000 independent realizations is exceptionally demanding computationally. Therefore, we first deploy our massive-scale simulation resources (L up to 192) for representative values of k ($k = 1, 2, 8, 32$) to rigorously characterize the phase transition behaviors in the thermodynamic limit. Specifically, for each parameter set (L, k, host model), we performed 20 000 independent simulations, tracking the exact algorithmic step of the giant component formation to achieve $O(1/M)$ resolution across over 1.2 million thermodynamic trajectories. We then utilize the smaller system sizes ($L =$ 1–10) to perform a high-density parameter sweep across all $k = 1, 2, 3, \ldots, 31, 32$, again with 20 000 independent simulations for each setup. This allows us to systematically locate the nonmonotonic behavior of the rigidity gap and identify the optimal choice parameter. Statistical analysis, including bootstrapped t tests [58] for the rigidity gap, is detailed in Secs. S6–S7 and Tables S1–S3 of the Supplemental Material [32]. The results presented below reveal the key physical behaviors and motivate the theoretical framework developed in the subsequent section.

In our analysis, we track several key quantities to characterize the transitions. The order parameter for connectivity is the relative size of the largest component, $S_{\max}/N$, where $S_{\max}$ is the number of vertices in the largest connected component and $N = (L+1)^3$ is the total number of vertices in the system. We monitor the peak susceptibility $\chi'_{L,\max}$ (as formally defined in Definition 9), which serves as the primary quantity for our FSS analysis. To locate the transition point, we measure the exclusive susceptibility χ'_L, whose peaks serve as reliable estimators for the critical thresholds.

A. Explosive connectivity transition for $k > 1$

We first present numerical results with L up to 192 for the connectivity transition in the 3D cubic lattices. In Figs. 3(a) and 4(a), we plot the order parameter $S_{\max}/N$ as a function of link density p for $k = 1, 2, 8, 32$ for a large system size of $L = 192$ [with $N = (L+1)^3 \approx 7\times10^6$] and compare the transitions.

For $k = 1$, both the NN and Intra models exhibit a gentle, continuous-looking curve characteristic of standard percolation. Note that the standard Achlioptas process with a choice parameter of $k = 1$ is equivalent to classical random percolation. For our NN host model, this corresponds to standard bond percolation on the simple cubic lattice. The critical threshold for this transition is a well-established numerical value, $p_c^{\text{cubic}} \approx 0.248\,81$ [5,59]. Our numerical results for the $k = 1$ case are in excellent agreement with this benchmark, validating our simulation framework. It is worth noting that this lattice threshold is higher than the mean-field prediction of $p_c(d) = 1/(d-1)$ for random d-regular graphs, which for $d = 6$ yields $p_c = 0.2$ [60], illustrating the role of the fixed lattice geometry in delaying percolation. This classical, continuous transition serves as a baseline against which we analyze the behavior for $k > 1$.

As k increases to 2 and 8, the transition becomes dramatically sharper. This occurs because the product rule, which minimizes the product of merging component sizes, becomes more effective with a larger pool of choices. It preferentially selects edges that connect small, isolated components, thereby suppressing the growth of a single dominant cluster and delaying the phase transition to a higher density. This suppression creates a "powder keg" of medium-sized components that eventually merge rapidly, leading to an explosive growth of the order parameter. While it has been established that this transition is formally continuous in the thermodynamic limit [14,18–20], our theoretical framework (detailed in Secs. S3 B and S3 C of the Supplemental Material [32]) demonstrates that for finite systems, a merger-cascade window exists where the order parameter exhibits a macroscopic jump. This phenomenon, often termed explosive percolation, manifests as an effective discontinuity for the system sizes relevant to mechanical metamaterials. The emergence of such abrupt jumps is a key feature of significant current interest in percolation theory; similar behaviors have been observed

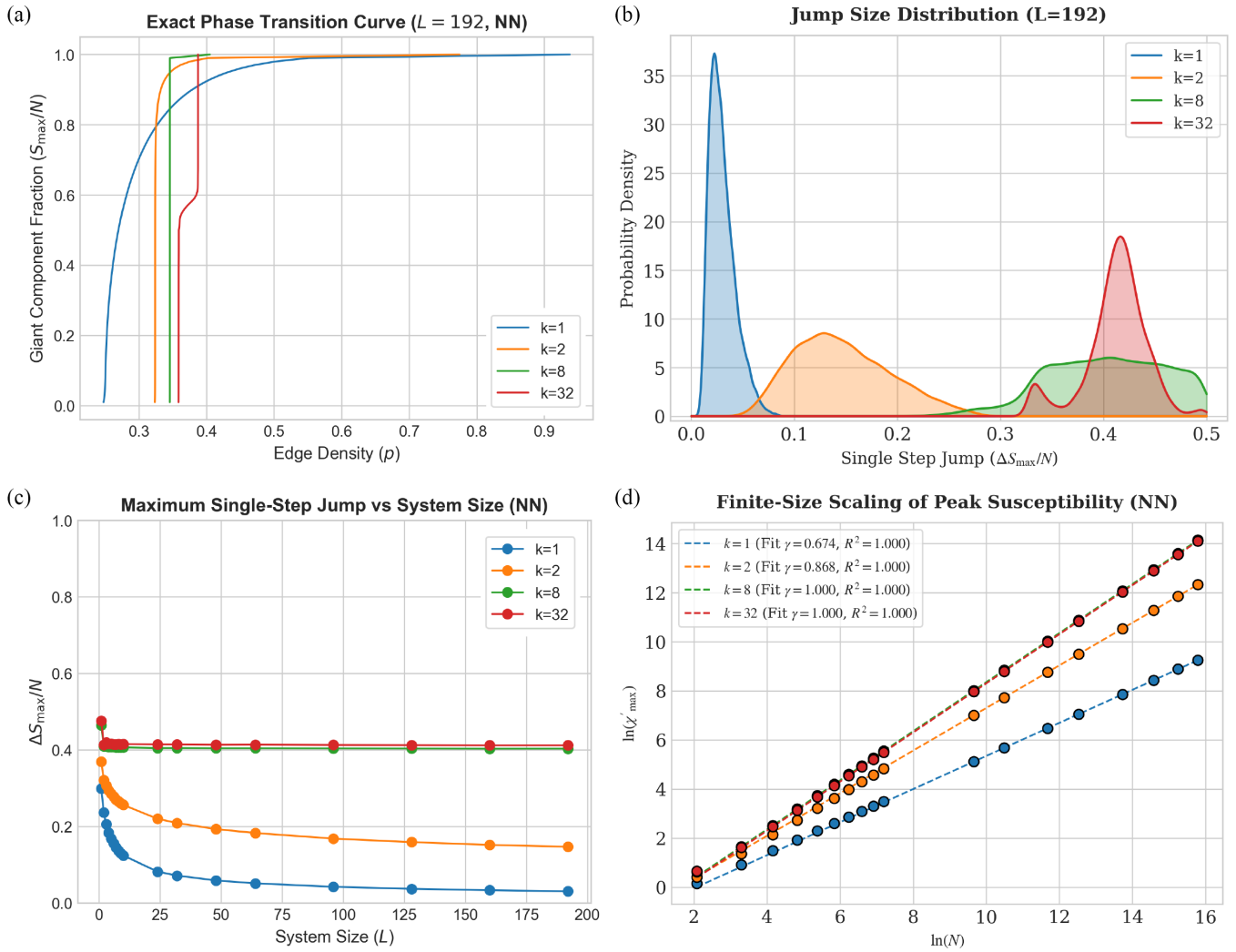


FIG. 3. Thermodynamic scaling analysis of the NN model. (a) High-resolution phase curves at $L = 192$ reveal a multiple-discontinuity cascade for $k = 32$. (b) The probability density of the single-step jump size at $L = 192$ demonstrates the transition from a continuous regime ($k = 1$) to an intermediate crossover plateau ($k = 8$) and finally a highly quantized, multimodal explosive regime ($k = 32$). (c) The maximum single-step jump $\Delta S_{\max}/N$ [where $N = (L + 1)^3$] stabilizes at a macroscopic fraction ($\sim$0.4) for large k, proving the discontinuity does not decay with system size. (d) Finite-size scaling of the peak susceptibility $\chi_{\max}$ demonstrates that for $k \geqslant 8$, the critical exponent mathematically converges to $\gamma = 1.000$, the signature of a first-order transition. Here, the dashed best-fit lines are computed strictly using data points for large system sizes ($L > 10$) to capture the true asymptotic scaling behavior.

in standard bond percolation on dense random graphs with prescribed degree sequences [61].

Interestingly, while the product rule enhances the efficiency of bond placement, one can see that it does not monotonically sharpen the transition in finite systems. As seen in Fig. 5, the transition for $k = 32$ is visually less abrupt than for $k = 8$ for all system sizes from $L = 1$ to $L = 192$. It contrasts sharply with processes that use globally informed "oracle" rules, such as the "most efficient" rule in the studies of origami and kirigami percolation [27,29], where a larger choice set always provides more options to a globally optimal decision process, leading to a monotonically sharpening transition. To explain this phenomenon, note that the k-choice product-rule Achlioptas process can be viewed as a deterministic process if k is sufficiently large. Now, if we consider the bond placement problem deterministically, then the optimal strategy under the product rule is to start by picking two isolated vertices (with product score $s = 1 \times 1 = 1$) at every step, until all N vertices in the system form $N/2$ pairs of vertices (connected components of size 2). After that, the optimal strategy will be to choose edges that connect two such connected components of size 2 as much as possible (with product score $s = 2 \times 2 = 4$), which can be repeated for $N/4$ steps. One can then continue the process until unavoidably getting one large cluster with size N. Therefore, performing the product rule deterministically (i.e., assuming that the maximum k) should yield a jump in $S_{\max}/N$ (from $2/N$ to $4/N$) at the link density $p = \frac{1}{2} \times \frac{N}{M}$, followed by another jump (from $4/N$ to $8/N$) at the link density $p = (\frac{1}{2} + \frac{1}{4}) \times \frac{N}{M}$ and so on. The structure will then become one large cluster at

$$p = \left(\frac{1}{2} + \frac{1}{4} + \frac{1}{8} + \cdots\right) \times \frac{N}{M} = \frac{N}{M}. \tag{1}$$

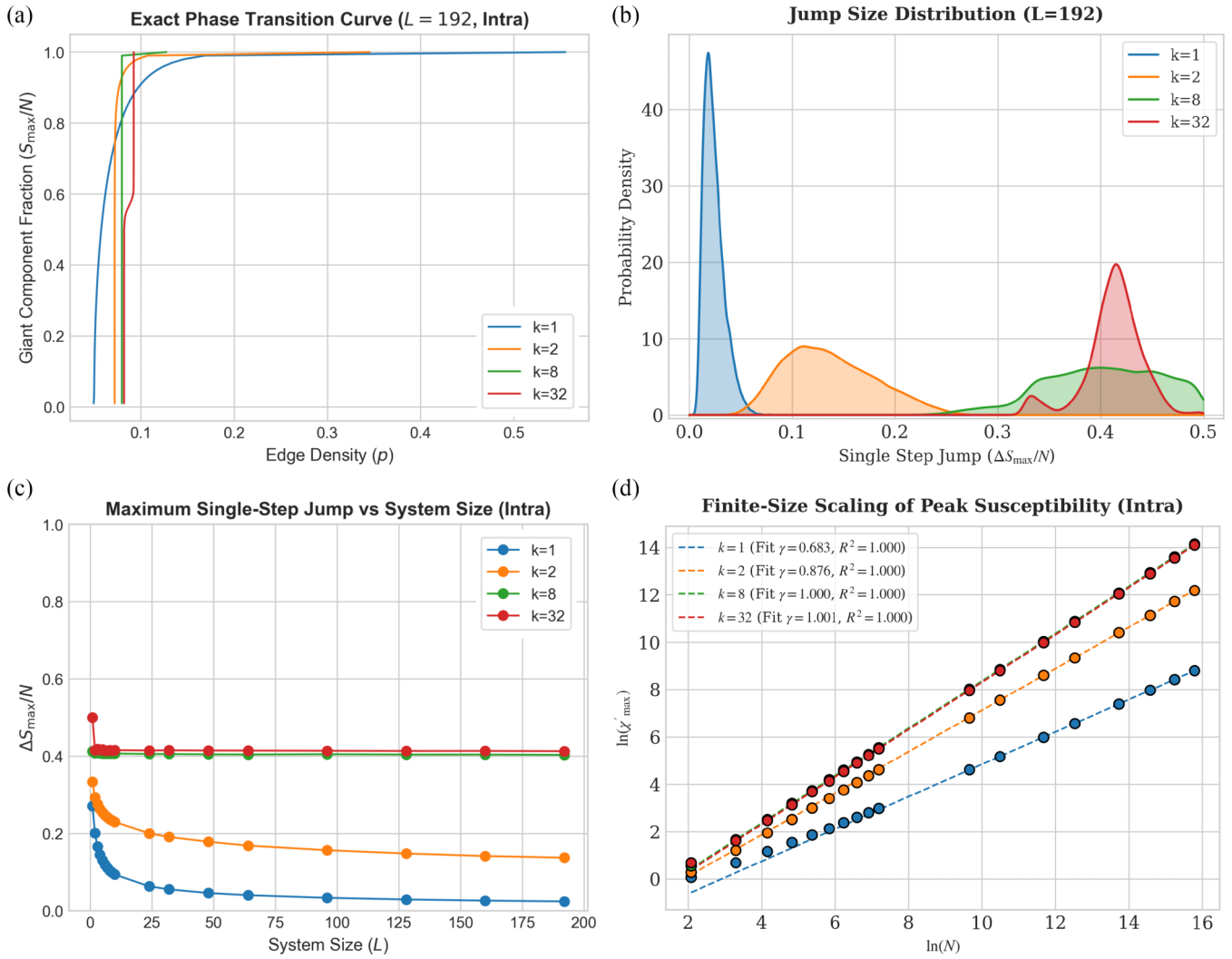


FIG. 4. Thermodynamic Scaling Analysis of the Intra model. Consistent with the NN model, the highly coordinated Intra lattice exhibits an explosive connectivity transition for $k \geqslant 8$. (a) The phase transition curves at $L = 192$ illustrate the severely delayed, abrupt onset of the giant component. (b) The probability density of the single-step jump size at $L = 192$ highlights the continuous regime ($k = 1$), the intermediate crossover plateau ($k = 8$), and the highly quantized, multimodal discontinuous regime ($k = 32$). (c) The maximum single-step jump establishes a persistent macroscopic fraction across all system sizes. (d) Finite-size scaling of the peak susceptibility confirms the critical exponent mathematically converges to $\gamma = 1.000$. Here, the dashed best-fit lines are computed strictly using data points for large system sizes ($L > 10$) to capture the true asymptotic scaling behavior.

This qualitatively matches the stepwise increase in $S_{\max}/N$ observed in the $k = 32$ plots for both NN and Intra models. However, note that in practice we will need $k \gg 32$ to match the above theoretical result quantitatively, as the total number of potential edges grows rapidly with L (e.g., even for only $L = 3$, we already have $M = 144$ for the NN model and $M = 468$ for the Intra model). Also, from the above argument, we can see that the theoretical transition width from $S_{\max} = 2$ to $S_{\max} = N$ will be

$$\frac{N}{2M} = \begin{cases} \frac{(L+1)^3}{2(3L^3+6L^2+3L)} & \text{for the NN model,} \\ \frac{(L+1)^3}{2(13L^3+12L^2+3L)} & \text{for the Intra model,} \end{cases} \quad (2)$$

and hence the transition for large k in practice may not be as sharp as the case of $k = 2$. A more detailed derivation of the required scale for k is included in Sec. IV B. See also Videos 3 and 4 of the Supplemental Material [32], in which we focus on smaller system sizes L and perform more high-density sweeps covering all $k = 1, 2, 3, \ldots, 31, 32$ to demonstrate the change in the transition behavior.

Simultaneously, the order parameter jump distribution $(\Delta S_{\max}/N)$ at the critical density provides a profound statistical signature of this transition. As observed in the jump size distribution for $L = 192$ in Figs. 3(b) and 4(b), the dynamics exhibit three distinct physical regimes. For $k = 1$, the jump size is predictably microscopic, forming a sharp unimodal peak near zero. For a larger number of choices (e.g., $k = 32$), the process avoids the giant component so aggressively that it induces a multiple-discontinuity cascade. This forces the jump distribution to exhibit quantized, multimodal peaks as a discrete number of macroscopic "megaclusters" are finally forced to merge. Crucially, the $k = 8$ case serves as the transition intermediate: The algorithm is strong enough to suppress standard continuous percolation but lacks the absolute control

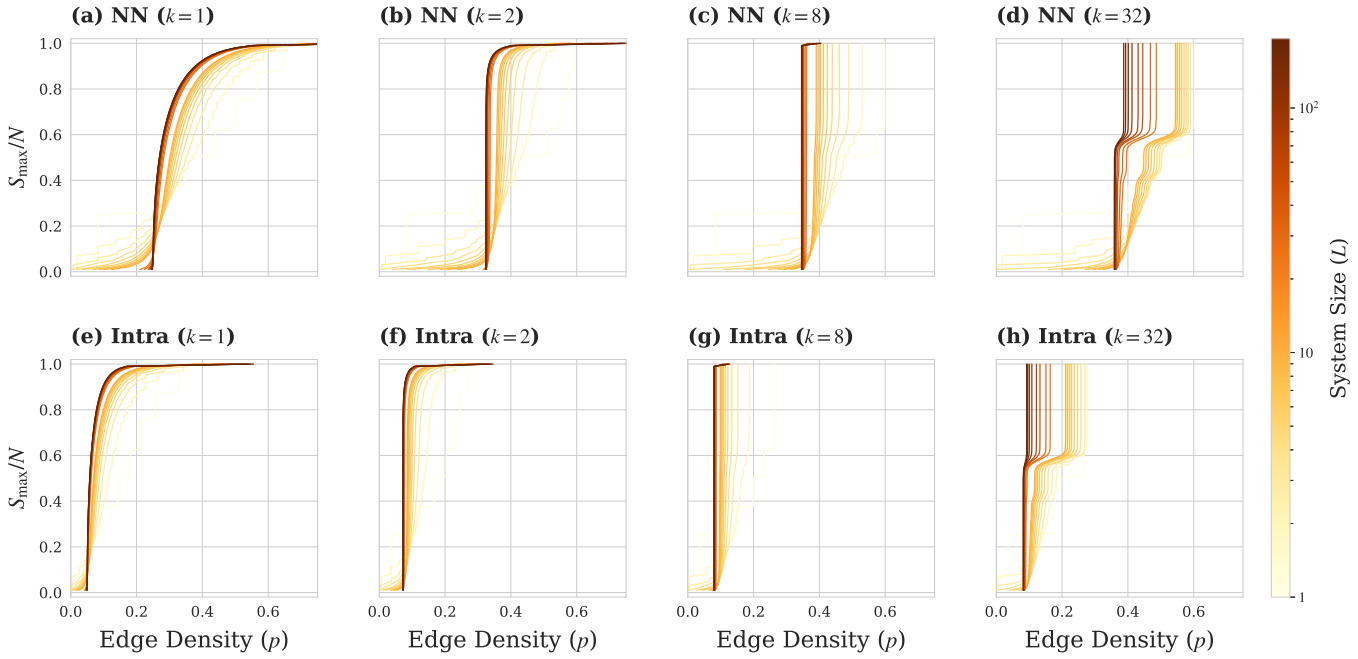


FIG. 5. Explosive connectivity transition phase curves for the NN and Intra models for system sizes up to $L = 192$. Here, we plot the normalized size S_{max}/N as a function of the link density p for the NN model [panels (a)–(d)] and the Intra model [panels (e)–(h)], evaluated across all system sizes up to $L = 192$. Each curve represents the average transition curve over the 20 000 simulations for a specific L.

required to enforce macroscopic symmetry. Consequently, the jump distribution is pushed down and smeared into a broad crossover plateau, perfectly capturing the onset of the explosive regime. In Figs. 3(c) and 4(c), we further plot the maximum single-step jump for different L from 1 to 192, from which we observe a persistent macroscopic fraction across different system sizes.

Further validation comes from the finite-size scaling of the peak susceptibility. While high-density parameter sweeps for small $L \leqslant 10$ (detailed in Sec. S7 of the Supplemental Material [32]) exhibit transient finite-size overshoots due to the onset of the merger cascade, our massive-scale simulation for large L (with L up to 192) definitively demonstrates that for $k \geqslant 8$, the scaling stabilizes and the critical exponent mathematically converges to $\gamma = 1.000$, confirming the strict theoretical maximum for a first-order jump [see Figs. 3(d) and 4(d), and Videos 1 and 2 of the Supplemental Material [32]].

It is natural to compare our 3D lattice findings with the recent study of explosive percolation in finite dimensions by Li *et al.* [18]. Investigating hypercubic lattices across dimensions $d = 2$–6 using an elegant event-based ensemble, Ref. [18] demonstrated that explosive percolation governed by the product rule remains formally continuous in the infinite thermodynamic limit, governed by standard finite-size scaling theory once dynamic fluctuations of the pseudocritical point are accounted for. Our results on the 3D simple cubic lattice (NN model) are fully consistent with this underlying thermodynamic continuity. At the same time, our work uncovers several distinct physical phenomena that extend beyond the scope of Ref. [18]. First, while Ref. [18] primarily characterized small choice parameters (principally $k = 2$), our broad exploration up to $k = 32$ reveals that the sharpening of the transition is nonmonotonic with choice number: intermediate choices ($k \approx 8$) produce a maximally abrupt crossover in finite systems, whereas very large choices ($k = 32$) approach a deterministic limit that spreads the merger cascade into discrete, quantized doubling steps. Second, beyond the nearest-neighbor cubic lattice, we examine the richly connected Intra cube geometry. Most importantly, while Ref. [18] focused exclusively on pure connectivity percolation, our work also studies the interplay between explosive connectivity and 3D mechanical rigidity, demonstrating how competitive link selection governs the closing of the rigidity-connectivity gap Δp_c. More details will be provided in the following sections.

B. Monotonic delay of connectivity with number of choices

In Fig. 6, we show the susceptibility plots for the NN and Intra models with different k. As k increases, the location of the susceptibility peak, which serves as a reliable estimator for p_c^{conn}, systematically shifts to higher densities for both the NN and Intra models across all investigated scales, from local system sizes up to our largest macroscopic limit of $L = 192$. Crucially, this delaying effect is not a transient finite-size artifact; the susceptibility peaks shift consistently to higher densities for every single system size L as k is increased, confirming that the delay persists in the thermodynamic limit. In our high-density parameter sweep for all $k = 1, 2, \ldots, 31, 32$ for smaller system sizes $L = 1, 2, \ldots, 10$ (Sec. S7 and Videos 5–8 of the Supplemental Material [32]), we further confirm that this observation is statistically robust: For the Intra model, a Spearman's rank correlation test between k and the measured p_c^{conn} yields a correlation coefficient of $\rho = 1.0$ ($p \ll 0.01$), signifying a perfect positive monotonic relationship.

This numerical observation provides powerful quantitative evidence for our further theoretical analysis. Our theoretical

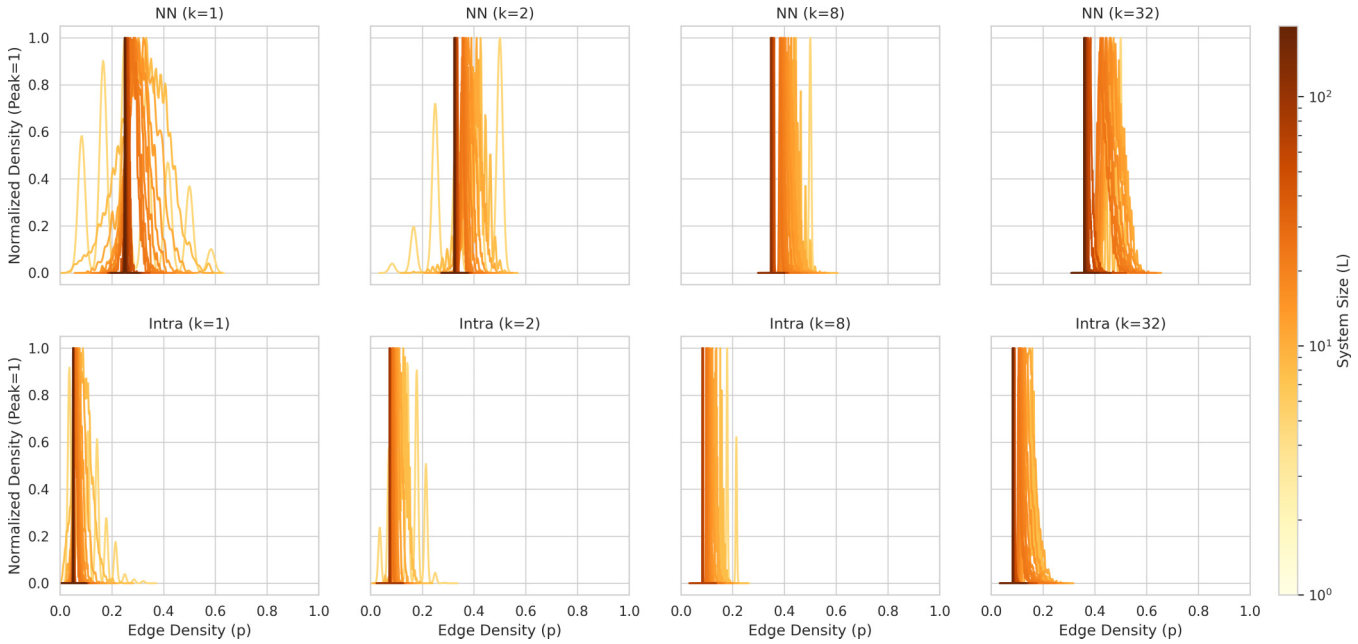


FIG. 6. Normalized exclusive susceptibility spectrum. The NN model (top row) and Intra model (bottom row) evaluated across all system sizes up to $L = 192$. To visualize the evolution across vastly different scales, the amplitude of each susceptibility curve, $\chi'_L(p)$ is normalized to a peak height of 1.0. As k increases, the peak systematically shifts to higher densities and sharpens, graphically illustrating the crossover to a first-order discontinuity. The color gradient maps to the system size L.

result in Theorem S3.40 of the Supplemental Material [32] proves that the connectivity threshold, p_c^{conn}, is a monotonically nondecreasing function of the number of choices k. In other words, greater choice consistently and predictably delays the onset of global connectivity.

C. Rigidity-connectivity gap and optimal efficiency

After considering the connectivity features of the NN and Intra models, we study the rigidity properties. As the NN lattice (coordination number $z = 6$) falls well below the Maxwell isostatic threshold for 3D rigidity, the NN model can never be rigid regardless of system sizes and number of choices. Therefore, here we focus on the rigidification process of the richly connected Intra model.

However, here we note that evaluation of 3D central-force rigidity for large system sizes poses a significant challenge computationally. While simple connectivity can be evaluated in almost-linear time, assessing 3D central-force generic rigidity is constrained by the nonlinear scaling of pebble game algorithms. The 3D relaxed pebble game requires extensive recursive searches to find and rearrange free pebbles. Near the rigidity transition threshold, nonlocal dependencies and redundant constraints trigger high rates of search failures and backtracking, causing the algorithmic complexity per trajectory to scale nonlinearly as $O(N^2)$ to $O(N^3)$, where $N = (L + 1)^3$ is the total number of vertices in the system. Because the number of vertices N scales cubically with the linear dimension L, the real-world execution timescales as $O(L^6)$ to $O(L^9)$, making the computation for large L infeasible.

Due to this prohibitive computational complexity of evaluating 3D relaxed rigidity on massive structures, here we focus on the smaller system sizes up to $L = 10$ ($N = (L + 1)^3 = 1331$) in the rigidity analysis, with a high-density parameter sweep for all $k \in [1, 32]$ and 20 000 simulations for each setup. To analyze the efficiency of rigidification, we consider the rigidity-connectivity gap Δp_c. This quantity measures the additional link density required to achieve a globally rigid state after a giant connected component has already formed. A smaller gap implies a more efficient rigidification process. Our numerical simulations reveal a dramatic initial increase in rigidification efficiency (a shrinking gap) that reaches an optimal minimum at intermediate k (see Table S3 of the Supplemental Material [32] for the complete k sweep from $k = 1$ to $k = 32$).

As seen in Fig. 7, for all values of k, a large and statistically significant positive gap ($\Delta p_c > 0$) exists between the connectivity transition (solid lines) and the rigidity transition (dashed lines) (see also Video 9 of the Supplemental Material [32]). The geometric basis for why this host supports efficient rigidity is explored later in Proposition S1.26 of the Supplemental Material [32]. More importantly, the dramatic initial shrinking of the gap provides strong motivation for our main theoretical result on local rigidification efficiency (Theorem 1). Furthermore, the gap's eventual plateau and slight widening at very large k ($k > 16$) beautifully align with our deterministic limit analysis (Sec. IV B). Here, our massive-scale simulations with 20 000 independent realizations for each L and each k offer a striking confirmation: As k increases, the rigidity-connectivity gap narrows rapidly to a global minimum at intermediate k before slightly widening at very large k. This sweep reveals that excessive choice leads to treelike, maximally floppy components, thereby yielding an optimal efficiency "Goldilocks" zone at intermediate k ($k \approx 16$). This provides compelling numerical evidence that the local product rule acts as a highly

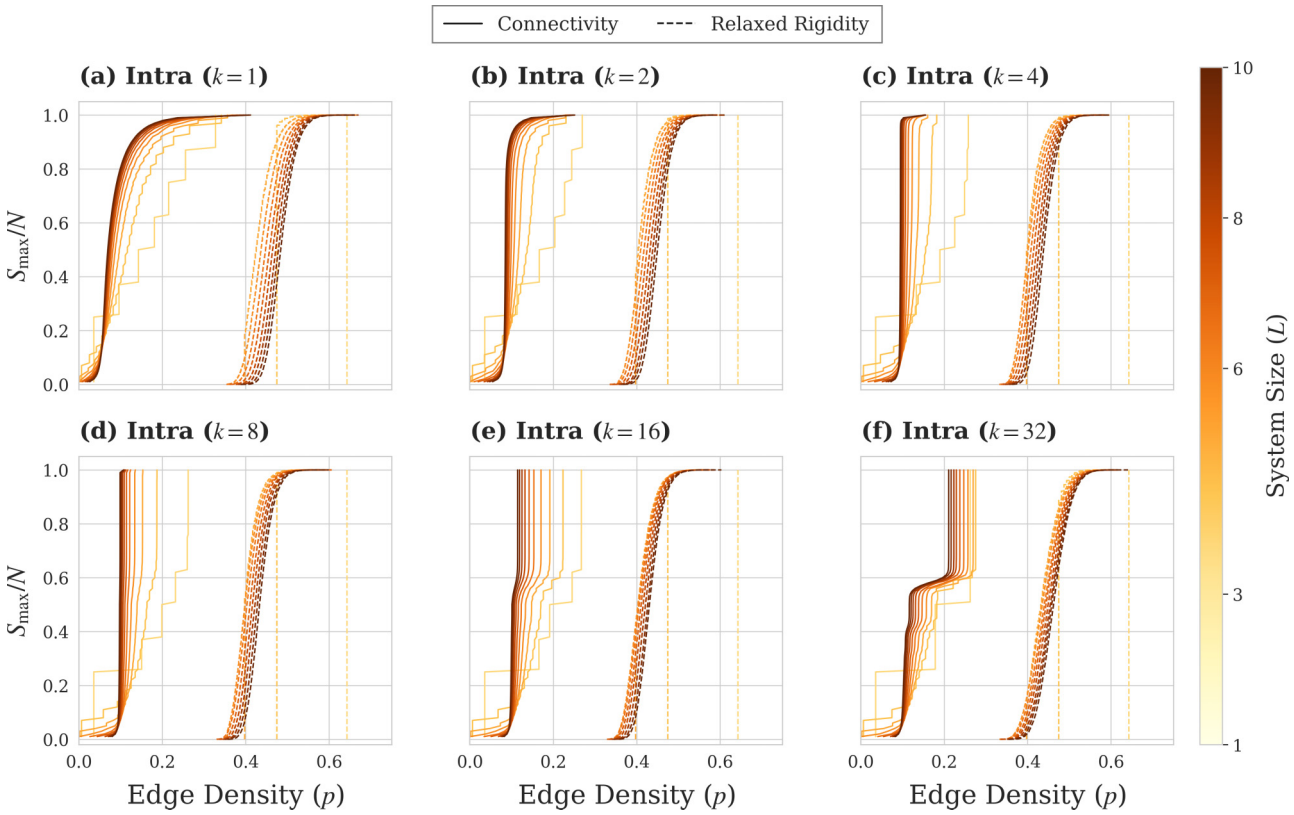


FIG. 7. Rigidity-connectivity gap up to macroscopic limits. We compare the connectivity transitions (solid lines) and relaxed rigidity transitions (dashed lines) via the normalized size S_{max}/N as a function of the link density p for the Intra model for $L = 1, 2, \ldots, 10$. All plotted curves represent exact ensemble averages over 20 000 independent realizations. Panels (a)–(f) correspond to $k = 1, 2, 4, 8, 16, 32$, respectively. A positive gap exists that systematically shrinks as k increases, proving that local choice monotonically enhances global rigidification efficiency. Notably, the relaxed rigidity thresholds exhibit clear inverse finite-size scaling: At small L, a high surface-to-volume ratio introduces numerous floppy surface modes requiring high bond density to stabilize, whereas for larger L, the bulk rigidifies earlier, shifting the dashed curves leftward. The color gradient maps logarithmically to the system size L.

effective proxy for achieving global mechanical stability efficiently. We remark that the underlying principle is that the Intra model, with its dense connectivity including face and body diagonals, serves as a strong "rigidity expander" [62], a class of graphs whose mechanical stability is governed by d-dimensional algebraic connectivity.

Analogous to the connectivity transition phenomenon discussed earlier in Sec. III A, we note that the sharpness of the rigidity transition in Fig. 7 appears maximal at an intermediate k (e.g., $k = 8$) instead of a much larger k (e.g., $k = 32$). This phenomenon can be explained by a similar deterministic argument. Specifically, as explained previously, the product rule with a sufficiently large k will preferentially form a large connected cluster at $p = N/M$, but the cluster will be floppy. As additional links are added at the subsequent steps, the size of the largest rigid cluster will increase steadily. This suggests that the rigidity transition for a large k may not be as sharp as that for an intermediate k.

It is important to contextualize our findings within rigorous mathematical results. Riordan and Warnke [14] proved that for any fixed k, the Achlioptas process undergoes a continuous phase transition in the strict thermodynamic limit ($N \to \infty$). However, this continuity can be physically elusive. Our extended massive-scale simulations reveal a clear physical bifurcation. While the onset of an "explosive" merger cascade begins at $k = 2$ (driving an initial anomalous finite-size scaling), the transition for low choice parameters ultimately remains continuous. Conversely, for $k \geqslant 8$, the finite-size corrections become so severe that the susceptibility scales with an exact exponent of $\gamma = 1.000$, which is the theoretical signature of a discontinuous jump. Furthermore, the single-step order parameter jump stabilizes at a macroscopic fraction regardless of system size. Thus, we classify the transition for $k \geqslant 8$ as "explosive connectivity", a mathematically continuous transition with such extreme finite-size corrections that it physically behaves as a first-order discontinuity in any realizable finite material structure.

IV. THEORETICAL FRAMEWORK AND ANALYSIS

Motivated by the observations from our numerical simulations, here we develop a series of theoretical results on explosive connectivity and rigidity.

A. Motivation: The rigidity-connectivity gap in mean-field models

While our primary focus is the Achlioptas process on a structured 3D lattice, we can gain valuable insights from simpler, analytically tractable mean-field random graph models, whose theory is detailed in modern treatments of

the subject [63]. These models offer a powerful conceptual baseline for understanding the fundamental relationship between network connectivity, coordination, and mechanical stability. While the theorems for these mean-field models do not directly translate to our lattice system, they provide a strong foundation for the hypotheses we develop and test in this work. Specifically, a detailed analysis of such models (provided in Sec. S2 of the Supplemental Material [32]) reveals a key principle: The gap between the connectivity and rigidity thresholds is a monotonically decreasing function of the average network coordination. This insight motivates our central hypothesis for how the choice parameter k influences rigidification in our lattice-based system.

By analogy with the mean-field results, we hypothesize that this effective coordination number, not k itself, is the fundamental parameter controlling the efficiency of rigidification

Hypothesis 1 (Effective coordination as the unifying principle). The primary role of the choice parameter k in the rigidity percolation of our 3D lattice models is to control the effective coordination at criticality, $d_{\text{eff}}(k)$. We hypothesize that the rigidity-connectivity gap, $\Delta p_c(k)$, is a monotonically decreasing function of this effective coordination number.

To make this connection explicit, we define the effective coordination at criticality as the average degree of the graph at the connectivity threshold: $d_{\text{eff}}(k) = 2|E(G^{\lfloor p_c^{\text{conn}}(k)M \rfloor})|/N = 2M p_c^{\text{conn}}(k)/N$. Since for our lattice models the total number of potential edges M is proportional to the number of vertices N, $d_{\text{eff}}(k)$ is directly proportional to the critical density $p_c^{\text{conn}}(k)$. Our theoretical result in Theorem S3.40 of the Supplemental Material[32] proves that $p_c^{\text{conn}}(k)$ is nondecreasing with k, establishing that $d_{\text{eff}}(k)$ is also nondecreasing.

This framework provides a powerful conceptual bridge: It suggests that even in a complex, history-dependent process on a fixed lattice, the fundamental mean-field principle—that higher coordination yields a smaller rigidity gap—still holds, with the Achlioptas rule acting as a kinetic dial to tune this coordination. This unifying principle is strongly validated by our numerical simulations for the Intra model (see Fig. 7 and Table S3 of the Supplemental Material [32]), where the gap shrinks dramatically from 0.4281 at $k = 1$ down to 0.3326 at $k = 16$ as the effective coordination is systematically increased.

Definition 14 (First-order scaling shift). The standard FSS relation for the shift of the pseudocritical point in a d-dimensional system is [64]

$$p_c(L) - p_c(\infty) = AL^{-d} + o(L^{-d}),$$

where A is a nonuniversal constant.

For the 3D cubic lattice structures studied here ($d = 3$), this predicts a shift proportional to L^{-3}. While we focus on the susceptibility scaling in our numerical analysis, this scaling shift provides an alternative, powerful method for identifying and characterizing first-order transitions in future studies.

B. Selection optimality, large-k effects, and bounds

A key observation from our numerical results in Sec. III A is that the sharpening of the phase transition is nonmonotonic with the choice parameter k; for instance, the transition appears more abrupt for $k = 8$ than for $k = 32$. This section develops a theoretical framework to explain this phenomenon by analyzing the conditions under which the stochastic Achlioptas process approaches a deterministic, globally optimal limit.

A deterministic process would, at each step, select an edge with the globally optimal (minimal) product score from the set of all available edges. Our stochastic process deviates from this ideal if none of the k sampled edges happen to be among this optimal set. We can formalize this "failure probability" and analyze how it depends on k.

Proposition 1 (Failure probability formula). Let M be the number of edges available for selection at a given step, m be the number of globally optimal edges among them, and k be the number of edges sampled uniformly at random without replacement. The probability that *none* of the k sampled edges is globally optimal equals

$$P(\text{fail} \mid k) = \frac{\binom{M-m}{k}}{\binom{M}{k}}, \tag{3}$$

for $0 \leqslant k \leqslant M$ (and interpreted as 0 if $k > M - m$).

Proof. This follows from a standard combinatorial argument on hypergeometric sampling. See Proposition S3.5 of the Supplemental Material [32].

Intuitively, increasing k should decrease this failure probability; Lemma S3.6 and Theorem S3.7 of the Supplemental Material [32] formalize this and prove that the improvement is strictly monotonic.

C. Theoretical model for local rigidification efficiency

We further develop a theoretical model to explain the central numerical observation that increasing the choice parameter k locally enhances the efficiency of mechanical rigidification, driving the initial shrinkage of the rigidity gap. Our model replaces heuristic arguments with a structured framework conditional on two physically-motivated assumptions. The analytical support for these assumptions is provided in Secs. S4 and S5 of the Supplemental Material [32]. Below, we first establish that the mechanical utility of an edge is a nonincreasing function of its local product-rule score. We then use this result within the synchronous coupling framework (Theorem S3.40 of the Supplemental Material [32]) to prove the main theorem on monotonic efficiency.

Let $(\mathcal{F}_t)_{t\geqslant 0}$ be the natural filtration generated by the k-choice process. Let $e = \{u, v\}$ be a candidate edge not in G_{t-1}. Its product score is $s(e) = |C_{t-1}(u)| \times |C_{t-1}(v)|$, and its rank gain is $\text{rgain}(e) \in \{0, 1\}$. We define the conditional progress function as follows:

Definition 15 (Conditional progress function). For any score value $s > 0$, we define the conditional progress function $P(s)$ as the expected rank gain of a uniformly chosen available candidate edge with score s:

$$P(s) := \mathbb{E}[\text{rgain}(e) \mid s(e) = s].$$

With the above definition, we can establish a monotonic relationship between score and redundancy:

Lemma 1 (Monotonicity of the conditional progress function). The conditional progress function $P(s)$ is a nonincreasing function of the score s.

Proof. See Sec. S5 of the Supplemental Material [32]. ■

With this Lemma rigorously established, we can now state and prove the following theorem.

Theorem 1 (Monotonic efficiency with choice). For the k-choice product-rule process, let $\mathbb{E}[\Delta\Phi_t^{(k)}]$ be the expected single-step progress toward rigidity at step t. For any $1 \leqslant k_1 < k_2$, we have

$$\mathbb{E}\big[\Delta\Phi_t^{(k_2)}\big] \geqslant \mathbb{E}\big[\Delta\Phi_t^{(k_1)}\big].$$

Consequently, the expected number of redundant edges added by any time T, $\mathbb{E}[N_{\mathrm{red}}(T;k)]$, is a nonincreasing function of k.

Proof. Conditional on the validity of the monotonic density assumption (Assumption S5.3 in the Supplemental Material [32]), the proof follows by combining the synchronous coupling from Theorem S3.40 in the Supplemental Material [32] with the resulting nonincreasing property of the conditional progress function $P(s)$.

For the score distribution, the synchronous coupling establishes that the minimal score selected by the k_2 process, $s^*_{k_2}$, is stochastically smaller than that selected by the k_1 process, $s^*_{k_1}$.

The expected single-step progress is $\mathbb{E}[\Delta\Phi_t^{(k)}] = \mathbb{E}_{s^*_k}[P(s^*_k)]$, where the expectation is over the distribution of the selected minimal score. From Lemma 1, the function $P(s)$ is nonincreasing. A standard result of probability theory is that for any nonincreasing function f and random variables X, Y where X is stochastically smaller than Y, it holds that $\mathbb{E}[f(X)] \geqslant \mathbb{E}[f(Y)]$.

Applying this principle with $f = P$, $X = s^*_{k_2}$, and $Y = s^*_{k_1}$, we immediately obtain

$$\mathbb{E}_{s^*_{k_2}}\big[P\big(s^*_{k_2}\big)\big] \geqslant \mathbb{E}_{s^*_{k_1}}\big[P\big(s^*_{k_1}\big)\big].$$

This inequality holds at every step t, which proves $\mathbb{E}[\Delta\Phi_t^{(k_2)}] \geqslant \mathbb{E}[\Delta\Phi_t^{(k_1)}]$.

Summing the expected progress over time shows that the total expected rank gain for k_2 is at least that for k_1. Since the number of redundant edges is $N_{\mathrm{red}}(T) = T - \sum_{t=1}^{T} \mathrm{rgain}(e_t)$, taking the expectation shows that $\mathbb{E}[N_{\mathrm{red}}(T;k)]$ is a nonincreasing function of k.

This result formally explains the dramatic initial shrinking of the rigidity-connectivity gap, Δp_c, with increasing k. As previously noted, for extremely large k, the topological shift toward spanning trees counterbalances this local efficiency, resulting in the global minimum observed at $k \approx 16$ as shown in Fig. 7.

V. CONCLUSION AND DISCUSSION

In this work, we have performed extensive numerical simulations and developed a rigorous framework to analyze explosive connectivity and rigidity in 3D cubic lattice structures. Our theoretical results establish a formal basis for the explosive signature of the connectivity transition. This is corroborated by massive-scale numerical simulations up to $L = 192$, which reveal that the peak susceptibility scales with an exact first-order exponent of $\gamma = 1.000$, and the transition features a persistent, macroscopic phase discontinuity characteristic of explosive percolation. For rigidity, our analysis on the richly connected Intra host shows the product rule optimally enhances the efficiency of rigidification pathways, finding a global minimum gap at intermediate k. Also, to explain the numerically observed initial enhancement of rigidification efficiency, we have introduced a novel conditional progress function. Our model formalizes the link between local selection rules and global mechanical stability. It shows that local efficiency follows from two physically motivated assumptions, for which we provide strong supporting evidence via tractable proxy models.

A. Broader impact and applications

The principles established in this paper offer a new lens through which to interpret phenomena in physical systems where connectivity and rigidity emerge. Specifically, while the k-choice product rule explicitly computes component sizes and requires global information, it serves as an effective *generative proxy* for nonlocal physical fields and history-dependent protocols in various scenarios discussed below.

1. Jamming in attractive particulate systems

Our model offers a mechanism to explain the distinct percolation behavior observed in jamming transitions. As shown by Lois *et al.* [65], attractive particulate systems exhibit two distinct transitions: a connectivity percolation at low density, followed by a rigidity percolation at a higher density. The region between these transitions represents a "floppy gel" state. Crucially, the mechanical state is highly history dependent; rapid quenching versus slow annealing leads to different structures.

In this context, the choice parameter k does not imply particles making calculations, but rather proxies the *thermodynamic protocol*. A standard random process ($k = 1$) mimics fast aggregation, resulting in a tenuous, floppy network (a large rigidity-connectivity gap). Increasing k mimics a slower, more energetically favorable pathway (annealing) that suppresses the growth of floppy dendrites. Our observation that increasing k shrinks the rigidity-connectivity gap aligns with the physical reality that optimized assembly protocols can delay the onset of a giant component to achieve a more mechanically stable (rigid) configuration more efficiently.

2. Biological network formation

The self-assembly of endothelial cells into functional vascular networks is a prime example of efficient percolation. While cells do not literally count the size of distant clusters, they interact via long-range substrate-mediated elastic interactions. Noerr *et al.* [66] demonstrated that contractile cells exert traction forces that create deformation fields in the substrate; these fields decay slowly, allowing cells to sense neighbors far beyond contact.

Crucially, the magnitude of the deformation field scales with the integrated contractility of the cell cluster. Therefore, a larger cluster generates a stronger mechanical signal. Our product rule, which favors merging smaller components to delay the formation of a giant cluster, phenomenologically captures the kinetic bias imposed by these long-range fields. The fields act as a physical proxy for "component size", driving the system toward a distributed, space-spanning network rather than a single dense aggregate. Our proof of monotonic

rigidification efficiency (Theorem 1) provides a formal basis for the observation that such mechanical guidance leads to more "cost-efficient" networks [66].

3. Design and fabrication of mechanical metamaterials

Finally, for mechanical metamaterials, our framework may serve as a design heuristic for top-down fabrication (e.g., 3D printing), rather than a model of self-assembly. In a manufacturing context, global component information is readily available.

Indeed, delaying the connectivity transition (p_c^{conn}) appears to generate a "less stiff" structure in the bulk sense. However, our objective is to optimize the efficiency of rigidification. In random assembly ($k = 1$), a giant component forms early but remains nonrigid (floppy) for a large range of density. This gap represents wasted material that contributes to mass but not stiffness. By increasing k, we suppress this early floppy percolation. When the structure finally connects, it does so at a density much closer to the rigidity threshold (a smaller Δp_c). Thus, our rule provides a prescription for fabricating disordered, porous architectures that achieve global rigidity with a minimum number of redundant bonds, maximizing the stiffness-to-weight ratio for stochastic lattice materials.

B. Future directions

This work opens several new avenues for research. The most immediate theoretical challenge is to provide a rigorous proof for the two central assumptions that underpin our rigidity framework: the monotonic average density of components and the emergent rigidity of large Intra host subgraphs. Progress on this front would likely require new analytical techniques to handle the history-dependent nature of the Achlioptas process.

Furthermore, our investigation highlights a major algorithmic hurdle in the study of finite 3D metamaterials. While the relaxed 3D pebble game effectively captures the macroscopic rigidification sequence, the strict generic $3N - 6$ constraint mathematically fails to manifest on finite cubic lattices with open boundaries due to severe surface floppy modes and localized geometric traps. Formulating an exact, computationally tractable combinatorial algorithm for strict 3D generic rigidity on bounded lattice geometries remains an outstanding open problem for future research.

Another compelling direction arises from our discovery of a nonmonotonic finite-size effect in the connectivity transition, where the apparent sharpness is maximized at an intermediate choice parameter (e.g., $k = 8$) functioning as a crossover regime. A systematic study of this optimal choice, $k_{\text{opt}}(L)$, and its dependence on system size and host geometry could yield deeper insights into the interplay between local heuristics and global phase transitions.

Finally, the predictive power of this framework invites its application to other classes of disordered materials, from amorphous solids to biopolymer networks, where the mechanisms of local selection and emergent stability remain open questions. The framework developed here offers a complementary perspective to data-driven machine learning approaches increasingly being used to study phase transitions [67], as well as to methods from topological data analysis, which use tools like persistent homology to characterize the multiscale structure, or "shape", of such complex systems [68].

ACKNOWLEDGMENT

This work was supported in part by the Croucher Foundation Startup Allowance and CUHK Faculty of Science Direct Grant for Research (to G.P.T.C.).

T.L.: Formal analysis, investigation, methodology, software, validation, visualization, writing–original draft; G.P.T.C.: Conceptualization, funding acquisition, investigation, methodology, project administration, supervision, writing–review and editing.

DATA AVAILABILITY

The simulation and analysis codes are available on GitHub at [69].

[1] D. Stauffer and A. Aharony, *Introduction to Percolation Theory* (Taylor & Francis, London, 2018).

[2] K. Christensen and N. R. Moloney, *Complexity and Criticality* (Imperial College Press, London, 2005), Vol. 1.

[3] M. Majewski and K. Malarz, Square lattice site percolation thresholds for complex neighbourhoods, Acta Phys. Pol. B **38**, 2191 (2007).

[4] N. A. M. Araújo, P. Grassberger, B. Kahng, K. J. Schrenk, and R. M. Ziff, Recent advances and open challenges in percolation, Eur. Phys. J. Spec. Top. **223**, 2307 (2014).

[5] Z. Xun and R. M. Ziff, Bond percolation on simple cubic lattices with extended neighborhoods, Phys. Rev. E **102**, 012102 (2020).

[6] M. Meloni, M. J. Large, J. M. González Domínguez, S. Victor-Román, G. Fratta, E. Istif, O. Tomes, J. P. Salvage, C. P. Ewels, M. Pelaez-Fernandez, R. Arenal, A. Benito, W. K. Maser, A. A. K. King, P. M. Ajayan, S. P. Ogilvie, and A. B. Dalton, Explosive percolation yields highly-conductive polymer nanocomposites, Nat. Commun. **13**, 6872 (2022).

[7] M. Sahimi, *Applications of Percolation Theory*, Applied Mathematical Sciences (Springer, Cham, 2023), Vol. 213.

[8] D. Achlioptas, R. M. D'Souza, and J. Spencer, Explosive percolation in random networks, Science **323**, 1453 (2009).

[9] R. M. Ziff, Explosive growth in biased dynamic percolation on two-dimensional regular lattice networks, Phys. Rev. Lett. **103**, 045701 (2009).

[10] R. A. da Costa, S. N. Dorogovtsev, A. V. Goltsev, and J. F. F. Mendes, Explosive percolation transition is actually continuous, Phys. Rev. Lett. **105**, 255701 (2010).

[11] F. Radicchi and S. Fortunato, Explosive percolation: A numerical analysis, Phys. Rev. E **81**, 036110 (2010).

[12] Y. S. Cho and B. Kahng, Suppression effect on explosive percolation, Phys. Rev. Lett. **107**, 275703 (2011).

[13] L. Yang and M. Li, Emergence of biconnected clusters in explosive percolation, Phys. Rev. E **110**, 014122 (2024).

[14] O. Riordan and L. Warnke, Explosive percolation is continuous, Science **333**, 322 (2011).

[15] H. K. Lee, B. J. Kim, and H. Park, Continuity of the explosive percolation transition, Phys. Rev. E **84**, 020101(R) (2011).

[16] R. M. D'Souza and J. Nagler, Anomalous critical and supercritical phenomena in explosive percolation, Nat. Phys. **11**, 531 (2015).

[17] R. M. D'Souza, J. Gómez-Gardeñes, J. Nagler, and A. Arenas, Explosive phenomena in complex networks, Adv. Phys. **68**, 123 (2019).

[18] M. Li, J. Wang, and Y. Deng, Explosive percolation in finite dimensions, Phys. Rev. Res. **6**, 033319 (2024).

[19] S. D. S. Reis, A. A. Moreira, and J. S. Andrade, Jr., Nonlocal product rules for percolation, Phys. Rev. E **85**, 041112 (2012).

[20] W. Choi, H. Chae, S.-H. Yook, and Y. Kim, Dimensional dependence of phase transitions in explosive percolation, Phys. Rev. E **90**, 022123 (2014).

[21] L. Asimow and B. Roth, The rigidity of graphs, Trans. Am. Math. Soc. **245**, 279 (1978).

[22] C. Moukarzel, An efficient algorithm for testing the generic rigidity of graphs in the plane, J. Phys. A: Math. Gen. **29**, 8079 (1996).

[23] J. Cheng and M. Sitharam, Maxwell-independence: A new rank estimate for the 3-dimensional generic rigidity matroid, J. Comb. Theor. Ser. B **105**, 26 (2014).

[24] D. J. Jacobs and B. Hendrickson, An algorithm for two-dimensional rigidity percolation: The pebble game, J. Comput. Phys. **137**, 346 (1997).

[25] A. Lee and I. Streinu, Pebble game algorithms and sparse graphs, Discrete Math. **308**, 1425 (2008).

[26] M. V. Chubynsky and M. F. Thorpe, Algorithms for three-dimensional rigidity analysis and a first-order percolation transition, Phys. Rev. E **76**, 041135 (2007).

[27] R. Li and G. P. T. Choi, Explosive rigidity percolation in origami, Proc. R. Soc. A **481**, 20240826 (2025).

[28] R. Li and G. P. T. Choi, Rigidity control of general origami structures, Commun. Phys. **9**, 217 (2026).

[29] G. P. T. Choi, L. Liu, and L. Mahadevan, Explosive rigidity percolation in kirigami, Proc. R. Soc. A **479**, 20220798 (2023).

[30] M. Li, J. Wang, and Y. Deng, Explosive percolation obeys standard finite-size scaling in an event-based ensemble, Phys. Rev. Lett. **130**, 147101 (2023).

[31] G. P. T. Choi, S. Chen, and L. Mahadevan, Control of connectivity and rigidity in prismatic assemblies, Proc. R. Soc. A **476**, 20200485 (2020).

[32] See Supplemental Material at http://link.aps.org/supplemental/10.1103/1fr3-bbxr for Videos 1–9 and a file containing movie descriptions, additional details on theoretical analysis, and experimental results, which includes Refs. [33–50].

[33] J. A. Tropp, An introduction to matrix concentration inequalities, Found. Trends Mach. Learn. **8**, 1 (2015).

[34] H. Duminil-Copin, Sharp threshold phenomena in statistical physics, Jpn. J. Math. **14**, 1 (2019).

[35] W. Perkins, Searching for (sharp) thresholds in random structures: Where are we now? Bull. Am. Math. Soc. **62**, 113 (2025).

[36] E. Friedgut and J. Bourgain, Sharp thresholds of graph properties, and the k-sat problem, J. Am. Math. Soc. **12**, 1017 (1999).

[37] A. Lew, E. Nevo, Y. Peled, and O. E. Raz, Sharp threshold for rigidity of random graphs, Bull. London Math. Soc. **55**, 490 (2023).

[38] M. Krivelevich, A. Lew, and P. Michaeli, Rigid partitions: From high connectivity to random graphs, J. Comb. Theor. Ser. B **175**, 126 (2025).

[39] Y. Peled and N. Peleg, On the rigidity of random graphs in high-dimensional spaces, Eur. J. Comb. **139**, 104460 (2027).

[40] M. Molloy and B. Reed, A critical point for random graphs with a given degree sequence, Random Struct. Algor. **6**, 161 (1995).

[41] M. Molloy and B. Reed, The size of the giant component of a random graph with a given degree sequence, Combinator Probab. Comp. **7**, 295 (1998).

[42] M. F. Thorpe and P. M. Duxbury, *Rigidity Theory and Applications* (Springer Science & Business Media, New York, NY, 2002).

[43] B. Bollobás, Random graphs, in *Modern Graph Theory*, Graduate Texts in Mathematics (Springer, New York, NY, 1998), Vol. 184, pp. 215–252.

[44] S. Boucheron, G. Lugosi, and P. Massart, *Concentration Inequalities: A Nonasymptotic Theory of Independence* (Oxford University Press, Oxford, 2013).

[45] Y. Xing and K. H. Johansson, Concentration in gossip opinion dynamics over random graphs, SIAM J. Control Optim. **62**, 1521 (2024).

[46] R. Durrett, *Probability: Theory and Examples*, Cambridge Series in Statistical and Probabilistic Mathematics (Cambridge University Press, Cambridge, 2019), Vol. 49.

[47] P. Grassberger, C. Christensen, G. Bizhani, S.-W. Son, and M. Paczuski, Explosive percolation is continuous, but with unusual finite size behavior, Phys. Rev. Lett. **106**, 225701 (2011).

[48] H. Chae, S.-H. Yook, and Y. Kim, Explosive percolation on the Bethe lattice, Phys. Rev. E **85**, 051118 (2012).

[49] Y. S. Cho, Explosive percolation on the Bethe lattice is ordinary, Eur. Phys. J. B **97**, 58 (2024).

[50] M. Olvera-Cravioto, Strong couplings for static locally tree-like random graphs, J. Appl. Probab. **59**, 1261 (2022).

[51] J. E. Graver, B. Servatius, and H. Servatius, *Combinatorial Rigidity*, Graduate Studies in Mathematics (American Mathematical Society, Providence, RI, 1993), Vol. 2.

[52] D. Garamvölgyi, S. J. Gortler, and T. Jordán, Globally rigid graphs are fully reconstructible, Forum Math. Sigma **10**, e51 (2022).

[53] G. Laman, On graphs and rigidity of plane skeletal structures, J. Eng. Math. **4**, 331 (1970).

[54] J. Cruickshank, B. Jackson, T. Jordán, and S.-I. Tanigawa, Rigidity of graphs and frameworks: A matroid theoretic approach, in *Surveys in Combinatorics 2026*, London Mathematical Society Lecture Note Series, edited by A. Gagarin, R. Behrend, M. Lettington, and I. Aliev (Cambridge University Press, Cambridge, 2026), Vol. 505, pp. 189–230.

[55] N. Javerzat and D. Notarmuzi, Fast algorithm for 2D rigidity percolation, Phys. Rev. X **16**, 031032 (2026).

[56] M. Lu, Y. Song, Q. Shi, M. Li, and Y. Deng, Dynamic Monte Carlo study of rigidity percolation using an event-based ensemble approach, Phys. Rev. E **113**, 064141 (2026).

[57] K. Binder, Finite size scaling analysis of Ising model block distribution functions, Z. Phys. B **43**, 119 (1981).

[58] B. Efron, Bootstrap methods: Another look at the jackknife, in *Breakthroughs in Statistics*, Springer Series in Statistics, edited by S. Kotz and N. L. Johnson (Springer, New York, NY, 1992), pp. 569–593.

[59] M. E. J. Newman and R. M. Ziff, Fast Monte Carlo algorithm for site or bond percolation, Phys. Rev. E **64**, 016706 (2001).

[60] A. Goerdt, The giant component threshold for random regular graphs with edge faults, Theor. Comput. Sci. **259**, 307 (2001).

[61] L. Lichev, D. Mitsche, and G. Perarnau, Percolation on dense random graphs with given degrees, J. Comb. Theor. Ser. B **167**, 250 (2024).

[62] A. Lew, E. Nevo, Y. Peled, and O. E. Raz, Rigidity expander graphs, Combinatorica **45**, 24 (2025).

[63] A. Frieze and M. Karoński, *Introduction to Random Graphs* (Cambridge University Press, Cambridge, 2015).

[64] K. Binder and D. P. Landau, Finite-size scaling at first-order phase transitions, Phys. Rev. B **30**, 1477 (1984).

[65] G. Lois, J. Blawzdziewicz, and C. S. O'Hern, Jamming transition and new percolation universality classes in particulate systems with attraction, Phys. Rev. Lett. **100**, 028001 (2008).

[66] P. S. Noerr, J. E. Zamora Alvarado, F. Golnaraghi, K. E. McCloskey, A. Gopinathan, and K. Dasbiswas, Optimal mechanical interactions direct multicellular network formation on elastic substrates, Proc. Natl. Acad. Sci. USA **120**, e2301555120 (2023).

[67] P. Mehta, M. Bukov, C.-H. Wang, A. G. Day, C. Richardson, C. K. Fisher, and D. J. Schwab, A high-bias, low-variance introduction to machine learning for physicists, Phys. Rep. **810**, 1 (2019).

[68] R. Ghrist, Barcodes: The persistent topology of data, Bull. Am. Math. Soc. **45**, 61 (2008).

[69] T. Lau and G. P. T. Choi, Explosive connectivity and mechanical rigidity in cubic lattice structures, GitHub, 2026, https://github.com/garyptchoi/cubic-lattice-percolation.